Next Materials 9 (2025) 101125

Contents lists available at ScienceDirect

Next Materials

journal homepage: www.sciencedirect.com/journal/next-materials

Research article

Photoactivated phenothiazine compounds convert sulfur-dyed cellulose fiber fabrics into microbicidal materials

Lilian Martins-Nascimento [a], Carin Cristina S. Batista [a], Luiza F. Sobrinho [a], Juliana D. Bronzato [b], Martha T. Oliveira [a], Karina P.M. Frin [a], Adrianne M.M. Brito [a], Silgia A. Costa [c], Sirlene M. Costa [c], Otaciro R. Nascimento [d], Iseli L. Nantes [a,*]

[a] Centro de Ciências Naturais e Humanas (CCNH), Universidade Federal do ABC, Santo André, SP, Brazil
[b] Faculdade de Odontologia de Piracicaba, Universidade Estadual de Campinas, Piracicaba, SP, Brazil
[c] Escola de Artes, Ciências e Humanidades, Universidade de São Paulo, Brazil
[d] Instituto de Física de São Carlos, Universidade de São Paulo (USP), São Carlos, São Paulo, Brazil

ARTICLE INFO

Keywords:
Phenothiazines
Photochemistry
Self-disinfecting fabrics
Sulfur black dye

ABSTRACT

Photoactivated phenothiazines with UV and visible light are converted to radical cations that remain stable for days. Recently, it was discovered that 10H-phenothiazine, when impregnated into natural and synthetic fiber fabrics, imparts antimicrobial properties to these materials. This study, for the first time, investigated the microbicidal properties of an industrial phenothiazine-based dye, sulfur black (SB), which is widely used in the fabric dyeing industry. Fluphenazine (FP), known for its ability to form stable cation radicals, was used as a comparative model. In 100 % cotton fiber fabric (100 C), SB and FP were converted to the corresponding cation radical species, effectively eliminating inoculated coronaviruses and bacteria. In 100 C, FP was more efficient as an antimicrobial agent than SB. Although both compounds generated cation radical species in the fabrics, only FP could produce singlet oxygen. The ability to generate singlet oxygen that can travel over distances contributed to the superior efficacy of FP. Consistently, 100 C treated with FP exhibited greater reactivity with phosphatidylcholine liposomes, a model for biological membranes. Notably, the virucidal activity of FP-treated fabrics persisted even after washing, showing the stability of the antimicrobial effect. MTT assays confirmed that the microbicidal action of FP- and SB-treated fabrics was not due to cytotoxicity, as cell viability remained above the threshold defined by ISO 10993-5. Thus, if microbicidal action is desired, SB-dyed 100 C should be used instead of 100 C. This study contributes to the design of new dye structures that integrate industrial dyeing capacity with effective microbicidal action.

1. Introduction

The advent of the COVID-19 pandemic and the increase in superresistant bacteria have led to growing interest in self-disinfecting materials. Various studies on fabric modifications for microbicidal action use metals and metal oxides, salts, quaternary ammonium compounds, graphene-based materials, and photosensitizers. Metals and metal oxides, such as silver, copper, and zinc, are notable for their potent antimicrobial and antiviral properties, including against SARS-CoV-2; however, their use may lead to toxicity, allergic reactions, and a loss of effectiveness after washing due to ion release. Salts like NaCl offer the advantage of enhancing filtration and inactivating microorganisms through osmotic pressure, but they can be easily washed off the mask, reducing the durability of the effect. Quaternary ammonium compounds offer broad biocidal action and are easy to apply; however, they may cause skin irritation, generate toxic residues, and promote the emergence of resistant microorganisms. Graphene-based materials are notable for their superhydrophobicity, self-cleaning properties, and local heat generation for disinfection. However, they require more complex manufacturing methods and still lack long-term safety assessments. Finally, photosensitizers such as TiO_2 and conjugated polymers have the advantage of producing reactive oxygen species (ROS) under light exposure, enabling efficient self-disinfection [1,2]. However, their activity is light-dependent and becomes ineffective in dark environments. Interestingly, a study involving 10H-phenothiazine, a photosensitizer, demonstrated that its virucidal effect on fabric persisted even

* Corresponding author.
E-mail addresses: ilnantes@ufabc.edu.br, ilnantes@ufabc.edu.br (I.L. Nantes).

https://doi.org/10.1016/j.nxmate.2025.101125
Received 12 November 2024; Received in revised form 13 August 2025; Accepted 22 August 2025
Available online 29 August 2025

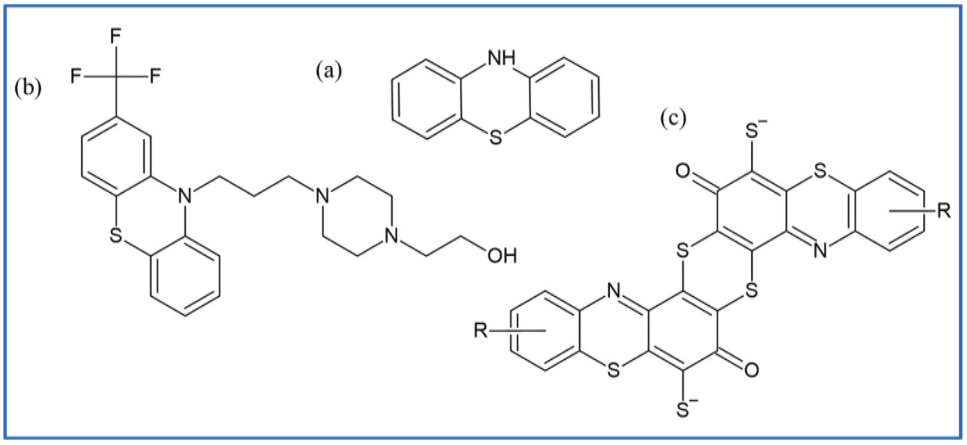

Fig. 1. The molecular structure of (a) phenothiazine nucleus, (b) fluphenazine, and the most probable structure of sulfur black that was used in this study, (c). R =NH or H.

without constant irradiation or after washing [3]. Furthermore, the microbicidal properties of industrial dyes have not yet been investigated. Based on this, the present work aims to investigate whether other phenothiazines exhibit similar microbicidal potential, focusing on the use of thiazine-based dyes already employed in industry (such as Sulfur Black) and exploring the potential for developing new phenothiazine-based dyes [4–6].

The phenothiazines (PTZs) are a significant group of photosensitizers bearing a phenothiazine nucleus constituted by two phenyl rings bound by sulfur and nitrogen atoms, as shown in Fig. 1. PTZs have diverse applications in medicine [4], dye industry [5], advanced materials [6], and more recently, as photosensitizers against the virus [3].

Rodrigues et al. characterized the photochemical behavior of the antipsychotic drugs thioridazine (TR), trifluoperazine (TFP), and fluphenazine (FP) modulated by the aggregation state of the molecules [7]. When phenothiazines are promoted from the ground state (S_o) to the singlet-excited state (S_1), they are converted to the triplet state by the intersystem crossing (ISC) mechanism. The S_1 state can also decay thermally or radioactively by fluorescence. The long-lived excited triplet state generated by ISC (lifetime of μsec) can survive long enough to conduct a photochemical reaction. In an aggregated state, a triplet state of phenothiazine can be deactivated by oxidizing the neighboring pair to a cation radical (Type I mechanism) [7]. The decay from T_1 can also occur by energy transfer to molecular oxygen, generating singlet oxygen ($^1O_2$) (Type II mechanism). Without oxygen and in solid matrices, triplet PTZs can decay to S_0 by phosphorescence [8,9]. Phenothiazines possess many new and fundamental biological properties, such as antibacterial, antiviral, anticancer, antiprotozoal, and multidrug resistance reversal activity [10,11]. The phenothiazine moiety is also present in low-cost sulfur dyes, including phenothiazonethioanthrone chromophore (sulfur black, abbreviated as SB), which is used to color cellulosic fibers [12–15]. This dye belongs to the sulfur dyes class that are generally known to be complex mixtures of molecular species containing a large proportion of sulfur in the form of sulfide (–S–), disulfide (–S–S–), and polysulfide (–S_n–) links and heterocyclic rings, especially the benzothiazole, thiazone and thianthrene ring systems. The Color Index recognizes at least 12 dyes named Sulfur Black. After simulating the EPR spectrum shown in the results, it was concluded that the structure that best matches the dye used is the one presented in Fig. 1c [16].

Fabrics enhanced with photoactive materials have the potential to directly and indiscriminately affect the structure of viruses and bacteria via photocatalytic and photothermal processes [2,17,18]. The production of pro-oxidant species through photocatalysis and the elevation in temperature via photothermal mechanisms result in microbial inactivation through disruption of the lipid membrane [3], damage to genetic material [19,20], and denaturing proteins [17,20]. Considering that previous studies demonstrated the virucidal action of 10HPHT, it was important to extend these investigations to other PTZ structures and establish a correlation between microbicidal action and the generation of pro-oxidant species. Also, the photoactivated microbicidal action of industrial dyes was yet another gap in the literature. Photosensitizers destroy pathogenic agents by generating pro-oxidant species through type I and II mechanisms. FP was selected as a model compared to SB to establish a correlation between the PTZ structure and the antimicrobial properties of these compounds in fabrics. This study can provide insights for developing efficient new antimicrobial fabric dyes based on photodynamic action.

2. Experimental

2.1. Materials

Fluphenazine dihydrochloride (FP), deuterium oxide (D_2O), acetonitrile, and chloroform were purchased from Sigma-Aldrich. Phosphatidylcholine Egg (PC) was purchased from Avanti Polar Lipids LLC. All aqueous solutions were prepared with deionized water (mixed bed of ion exchangers, Millipore). Flat fabric with 100 % cotton composition and a grammage of 101.73 g/m^2 (100 C). 100 % cotton fabric dyed with sulfur black was kindly donated by EACH/USP.

2.2. Generation and characterization of cation radicals from FP and SB in natural and synthetic fiber fabrics

2.2.1. Generation of stable free radicals of FP and adsorption in fabrics

For the experiment, 20 ml aqueous solutions of FP at 1-, 8-, and 13-mM concentrations were prepared. Cotton fabrics, cut into 2 × 2 cm squares, were immersed in the solutions with constant agitation and irradiated using a 254 nm UV-C lamp (75 W) for 30 min at a 10 cm distance. After irradiation, samples were agitated and dried with nitrogen gas under room light. The cotton fiber fabric samples impregnated with FP under irradiation are named 100 C+FP and contain the radical cation since it remains stable for days.

2.2.2. Generation of SB radical cation in cotton fabric

The 100 C dyed with SB was a donation produced using an industrial method described in the supplementary material. A 2 × 2 cm piece of sulfur black-dyed 100 C was irradiated with the UV-C lamp in the same conditions as FP-impregnated samples. The SB radical cation is also stable and remains at 100 C after irradiation for days. These samples are referred to as 100 C + SB.

2.2.3. Determination of singlet oxygen formation

To study the photochemical mechanism, 100 C+SB and 100 C+FP pieces prepared as described above were placed inside a cuvette filled with chloroform. Singlet oxygen generation was monitored at 1270 nm using a Hamamatsu Near Infrared (NIR) photomultiplier, which used as an excitation source a 375 nm diode laser (LDH-P-C-375B, PicoQuant GmbH) driven by a PDL 820 computer-controlled, all connected in a PicoQuant FluoTime 300.

2.2.4. Cotton fabric washing with household detergent

The cotton fabrics with FP and SB were washed with household laundry detergent with the following composition: linear alkyl benzene sodium sulfonate, sodium alkyl ether sulfate, buffering agents, pH-adjuster, thickeners, coadjutants, dye, enzyme, optical brightener, fragrance, anti-redeposition agent, isotiazolines, and preservants. The washing consisted of immersion of the cotton fabric piece in a Becker containing 50 ml of fresh water, in which the amount of detergent prescribed by the manufacturer was added according to the mass of clothes used for washing. The cotton piece was shaken for 10 min and rested in the same detergent solution for 50 min. In the following, the cotton piece was submitted to three cycles of rinsing with fresh water for 10 min. After washing, the cotton pieces were dried by purging N_2 before characterizations. These washed fabrics were used in the virucidal test to study whether the fabric retains its microbicidal properties even after washing.

2.2.5. UV-visible spectrometry

The UV−visible spectra were recorded from 200 to 1100 nm in an Evolution 220 UV–visible spectrophotometer (Thermo Fisher, USA). The FP solution was analyzed using 10 mm cuvettes, and all fabrics treated with FP and SB (before and after washing) were analyzed using the sphere integrator module.

2.2.6. Electron paramagnetic resonance (EPR) spectrometry

Pieces of the treated fabrics (100 C+FP and 100 C+SB) were placed in the tube for analysis, and EPR spectra were recorded at room temperature (EPR EMX 10–2,7 Plus, Bruker, Germany). At a frequency of about 9.4267 to 9.4406 GHz, three scans with a magnetic field range from 3470 to 3570 G were accumulated with 1023 data points each (conversion time 10.24 ms), microwave attenuation of 10 dB, and a field modulation amplitude of 1 and 5 T at 100 kHz modulation frequency.

2.2.7. Color fastness to washing and light according to textile standards

The color fastness test for washing was carried out by ISO 105-C06:2010. Textiles – Tests for color fastness. Part C06: Color fastness for *domestic and commercial laundering*. The method used was the AIS (simple test at 40°C). Fabric color change assessments were carried out by ISO 105-A02:1993 – *Textiles – Color fastness tests – Part A02: Grayscale for color change assessment*. The ISO-A03:1993 standard was used for color transfer evaluations as a basis – *Textiles – Color fastness tests – Part A03: Grayscale for stain evaluation* - The colorimetric coordinates in the CIEL*a* b* space, the color shift (ΔE) was measured using Konica Minolta cm-2600d spectrophotometer, under the D65 illuminant with 10º observer angle, 400–700 nm scan, and with the inclusion of specular reflection measurement and UV filter. The color fastness test for artificial light was performed by standard ISO 105-B02:2014 – Textiles - Tests for color fastness part B02 Color fastness for artificial light: Xenon arc fading lamp test.

2.2.8. Traction and elongation

The specimens measuring 6 × 18 cm, with the largest measurement in the longitudinal direction (warp), were stored at 20 ± 2 ∘C and relative humidity of 65 ± 4 % for 24 h. The tests were performed according to the ASTM D 3822 (2007) standard using a Universal Testing Machine “Instron” model 5869, with 2 N of pretension, 100 mm min^{-1} speed, and 200 mm distance. The tensile parameter was determined when the fiber yarn broke, immediately after maximum elongation. The test was conducted at the Textile Technology Laboratory of the Institute of Technological Research (LTT-IPT).

2.2.9. Air permeability

The air permeability test was performed in accordance with the ISO 9237:1995 standard, "Textile - Determination of the air permeability of fabrics." The test specimens measuring 15 × 15 cm were evaluated using an air permeability meter with electronic flow control FX 3300-III - Textest, with a 20 cm^2 clamping head and 3 3-range. The programmed pressure was 100 Pa, and the results were obtained in $L/m^2/s$ as the unit of measurement. The assay was performed at the Textile Technology Laboratory of the Technological Research Institute (LTT - IPT).

2.3. Microbicidal application

2.3.1. Cell viability

The MTT assay was used to evaluate the cytotoxicity of 100 C+FP and 100 C+SB by measuring cell viability, following ISO 10993-5:2009 standards, which define ≥ 70 % viability as non-toxic. Human lung fibroblast cells (MRC-5 line) were cultured in DMEM with supplements and maintained until 90 % confluence. After plating 10,000 cells per well and incubating for 24 h, cells were treated with the medium used to rinse the FP-impregnated 100 C and SB-dyed 100 C and incubated for another 24 h. MTT solution was then added, followed by a 4-h incubation, DMSO addition to dissolve formazan crystals, and absorbance measurement at 570 nm to assess viability, as reported in the literature [21]. The objective was to exclude the chemical toxicity of residues extracted from fabrics by rinsing. Considering that the impregnation of FP in fabrics is done by incubating the fabric in the phenothiazine solution under irradiation, the stable radical cation of FP should also be present in the fabric. SB absorbs visible light in all the visible spectral range, and radical cation can be formed even upon exposure to room light. Still, the sample was also UV-irradiated for this assay.

2.3.2. Viral inactivation assay

Virucidal assays were conducted using Human Coronavirus 229E (HCoV-229E) and MRC-5 lung fibroblast cells. One day prior, 20,000 cells were seeded per well in 96-well plates. Samples (1 cm^2) treated with FP and SB were exposed to 1000 ID_{50} of HCoV-229E for 5 min, then rinsed with culture medium, which was transferred to the cell wells. After 4 days of incubation at 37°C with 5 % CO_2, wells were imaged, and viral RNA was extracted for analysis. cDNA was synthesized, and qPCR was performed in triplicate targeting the ORF1 region to quantify remaining viral RNA. Reactions were run in duplicate for each replicate, and results were statistically analyzed using one-way ANOVA and Bonferroni’s post-test ($P < 0.001$), as described elsewhere [3].

2.3.3. Lipoperoxidation assay

An in-situ ATR-FTIR technique was employed to investigate the oxidation of phosphatidylcholine liposomes, simulating the lipid component of viral envelopes. Liposomes (14 mM L-α-Phosphatidylcholine) were incubated with 100 C+FP and 100 C+SB prepared as described in Sections 2.2.1 and 2.2.2. The samples were incubated in the liposome suspensions under visible light and agitation for 30 min. Afterward, cotton fabrics were washed with chloroform, and the lipid-containing solution was collected. The chloroform phase was separated and analyzed. For spectral analysis, 10 μL of each sample was applied to a diamond ATR crystal and dried. Infrared spectra were recorded using a Varian 640-IR spectrometer, processed from 64 scans at 4 cm^{-1} resolution. Spectra were referenced to air, analyzed with Varian Resolutions Pro software, and normalized and compared using Origin Pro 8.5. This method was adapted from Bronzato et al.

2.3.4. Mechanism of virus inactivation analyzed by EPR

The fabrics with FP and SB were analyzed in the EPR. Then, they

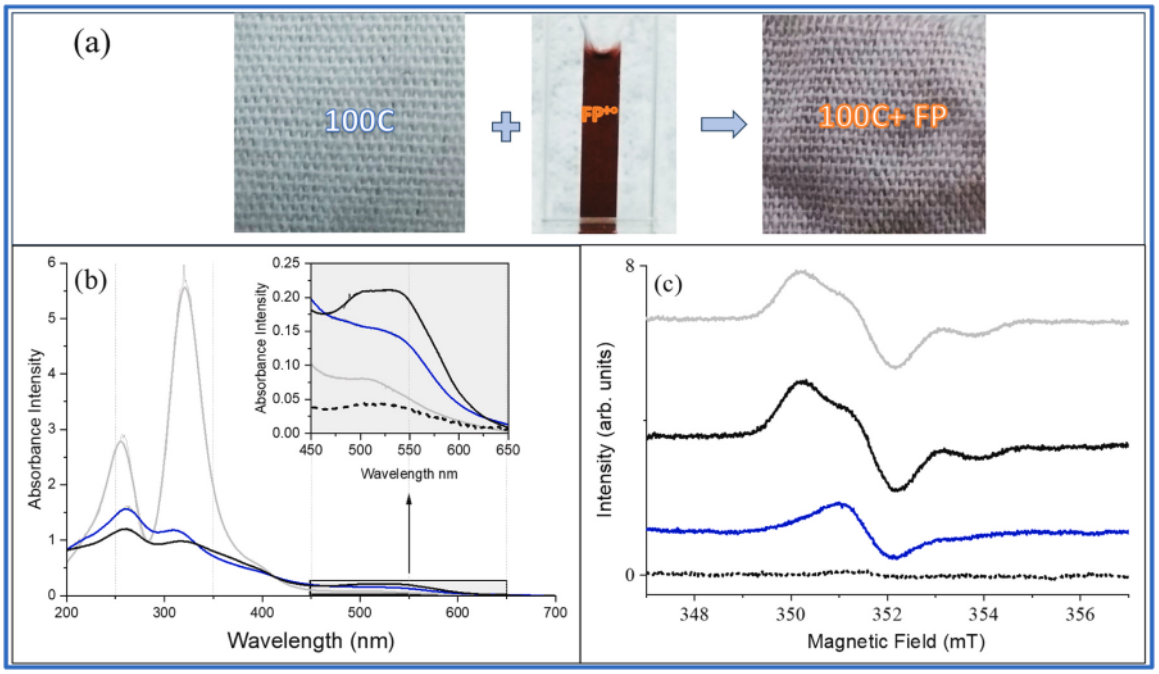

Fig. 2. (a) Photographs of 100 % cotton fabric (100 C), 100 C with irradiated fluphenazine (100 C+FP), and irradiated FP solution ($FP^{\bullet+}$). (b) UV–vis absorption spectra of FP solution (dotted line) and 100 C+FP at the concentrations of 1 (blue line), 8 (black line), and 13 mM (light grey line) - The spectra were subtracted for the fabric and background. (c) EPR spectra of 100 C+FP at the concentrations of 0 mM (dotted black line), 1 mM (blue line), 8 mM (black line), and 13 mM (light grey line).

were embedded in the egg Phosphatidylcholine (PC) liposome and analyzed again. Electron Paramagnetic Resonance Spectroscopy spectra were recorded at room temperature (EPR EMX 10–2,7 Plus, Bruker, Germany). At a frequency of about 9.4267 to 9.4406 GHz, three scans with a magnetic field range from 3470 to 3570 G were accumulated with 1023 data points each (conversion time 10.24 ms), microwave attenuation of 10 dB, and a field modulation amplitude of 1 and 5 T at 100 kHz modulation frequency.

2.3.5. *Antimicrobial inactivation assay*

The methodology was adapted from previous studies [22,23]. An inoculum (Escherichia coli ATCC 25922) was prepared in 20 ml of BHI broth (Brain Heart Infusion, Kasvi, Pinhais, PR, Brazil) and incubated for 24 h at 37°C. Then, the bacteria concentration was adjusted to 3×108 cells/ml, and a volume of 400 µL from the previous suspension was added to 20 ml of BHI broth and incubated for 2 h at 37°C. The bacteria concentration was measured again and diluted in BHI broth until it reached 150×10^6 cells/ml. 100 µL of this inoculum was added to 1×1 cm pieces of 100 C+FP and 100 C+SB fabrics, prepared as described above, and incubated at 37°C for the appropriate time. Subsequently, 10 ml of sterile physiological saline solution was added to the samples, and they were vortexed for 1 min. The number of live bacteria was assessed by the serial dilution plate count method using Macconkey agar plates (Kasvi, Pinhais, PR, Brazil), which were incubated for 24 h at 37°C. The test was performed in triplicate, and the average was used to analyze the result. To analyze the results, using 100 C as a negative

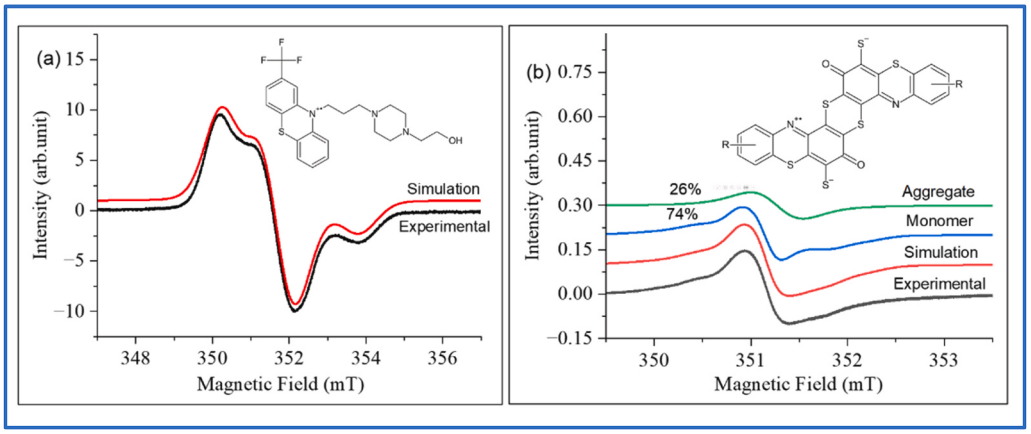

Fig. 3. Simulation of the EPR spectra using the HStrain program. (a) The black line corresponds to the experimental spectrum of 100 C+FP and the red line to the simulated spectrum; (b) The black line corresponds to the experimental spectrum of 100 C+SB after washing with water; the red line corresponds to the simulated spectrum; the blue line corresponds to the monomeric fraction of the SB radical cation; the green line to the aggregate fraction of the SB radical cation. The inset shows the structure of sulfur black.

Table 1
EPR parameters obtained for FP and SB free radicals.

Samples	g_1	g_2	g_3	$Lwpp_1$ (mT)	$Lwpp_2$ (mT)	A_1 (MHz)	A_2 (MHz)	A_3 (MHz)
100 C+FP	2.0077	2.0027	2.0053	0.853	0.0766	0.0	48.72	4.72
100 C+SB (monomeric)	2.0023	2.0062	2.0099	0.192	0.057	9.87	0.09	0.94
100 C+SB (aggregate)	2.0046	2.0053	2.0064	0.267	0.314			

Table 2
Color fastness results to light, after 30 h under light exposure.

Samples	Score after 30 h under light D65
100 C	4
100 C+FP	2–3*
100 C+SB	5

* Sample exhibited intensification of red color

control, Eq. 1 was used:

$$\frac{\text{number of bacteria on control fabric} - \text{number of bacteria on treated fabric}}{\text{number of bacteria on control fabric}} * 100 \quad (1)$$

3. Results and discussion

3.1. Impregnation and characterization of radical cations in cotton fabrics

When irradiated, an aqueous solution of FP (colorless) is converted to a red solution, which is characteristic of the formation of $FP^{\bullet+}$ (Fig. 2a).

A cotton fabric piece immersed in a red fluphenazine solution takes on a reddish color (Fig. 2a), and its absorption spectrum exhibits a band in the visible region at 520 nm that overlaps the band of $FP^{\bullet+}$ aqueous solution (zoomed inset of Fig. 2b). A piece of 100 % cotton fabric was impregnated with $FP^{\bullet+}$ photogenerated in FP solutions of 1, 8, and 13 mM to analyze the effect of FP concentration on the radical cation impregnation in 100 C. The samples of 100 C were immersed and irradiated in 0, 1, 8, and 13 mM of FP solutions and analyzed by UV–visible and EPR (Fig. 2b and c, respectively). Fig. 2b shows that the higher intensity of the band assigned to $FP^{\bullet+}$ was present in 100 C treated with the $FP^{\bullet+}$ solution. The corresponding EPR spectra showed spectral differences in the 100 C samples incubated in FP solution of 1 and 8 mM. These differences are probably related to the aggregation states of FP molecules in the cotton fabric weft. In contrast, the EPR signal was similar but slightly lowered in the sample incubated with the FP solution of 13 mM. Therefore, 100 C treated with an FP solution of 8 mM (100 C+FP) was chosen for subsequent characterizations and microbicidal application. A standard industrial protocol for dyeing 100 C with SB was used, and this sample was analyzed and applied as received.

The simulations of EPR spectra for 100 C+FP and 100 C+SB were consistent with the presence of $FP^{\bullet+}$ and $SB^{\bullet+}$ in 100 C with unpaired electrons in nitrogen (Fig. 3a and b, respectively).

In contrast to the EPR of $FP^{\bullet+}$, the spectrum of 100 C+SB reveals the presence of two populations of the radical, one more abundant, 74 % monomeric, and the other 26 % corresponding to the aggregate of the radical (Fig. 3b). The simulation of the EPR spectra using the HStrain program revealed that the spectrum has a nitrogen moiety associated with the following signal characteristics depicted in Table 1. Considering the diversity of possible structures of black dyes containing the phenothiazine moiety, the structure provided to the simulation software, which resulted in simulated spectra well-fitted to the experimental result, was chosen as the probable structure of the SB used in the present study.

The samples of 100 C+SB were submitted for testing to evaluate light exposure and washing fastness (Tables 2 and 3, respectively).

Table 2 shows that 100 C and SB-dyed 100 C resist color change by light exposure. The low score obtained by 100 C+FP results from the intensification of the red color, indicating an increase in $FP^{\bullet+}$ in the fabric.

Washing fastness analyzes the resistance to color removal and transfer by washing color-dyed fabrics together (Table 3). It is essential to analyze color fastness to determine the viability of washing different colored pieces together and the stability of the photosensitizers in the textile. Furthermore, since FP could be used as a temporary additive for non-disposable PPEs, it is essential to know if a reapplication is necessary after each washing.

Based on the grayscale, samples were evaluated before and after treatment or dyeing. The color transfer of the samples to the multifiber fabrics was analyzed on the color transfer scale. Grades were assigned to solidity grades 5, 4, 3, 2, and 1, and intermediate grades 4–5, 3–4, 2–3, and 1–2. A score of 5 equals no color change/transfer, and 1 equals excessive color change/transfer. In the grayscale, the fabric with SB had an almost imperceptible change when washed (4−5). Meanwhile, the fabric with FP showed a more noticeable change (1). The color variation between the fabric before and after washing, measured by the spectrometer, shows that industrial dyeing results in better fixation of SB (0.63) compared to FP (14.88). The coloring in the wash of the dyed fabrics (Table 3) was classified as “very good” (5) for all fibers of the multifiber fabric, except wool (4−5), in both fabrics evaluated [4], which shows that both FP and SB were satisfactorily impregnated the fabric.

Additionally, tests of tensile strength and air permeability were performed and are available in the Supplementary Material.

3.2. Virucidal application

The 100 C+FP and 100 C+SB were evaluated as self-disinfecting materials.

The treated fabrics and their corresponding control (100 C) were inoculated with human coronavirus 229E (HCoV-229E). HCoV-229E is

Table 3
Washing fastness of cotton fabrics.

Samples	Visual change grayscale	ΔE*	Color staining					
			Acetate	Cotton	Polyamide	Polyester	Acrylic	Wool
100 C+SB	4−5	0.63	5	5	5	5	5	4−5
100 C+FP	1	14.88	5	5	5	5	5	4−5

* Difference between the input content’s displayed color and the original color standard. The lower ΔE, the greater the accuracy, while the higher ΔE, the more significant the mismatch.

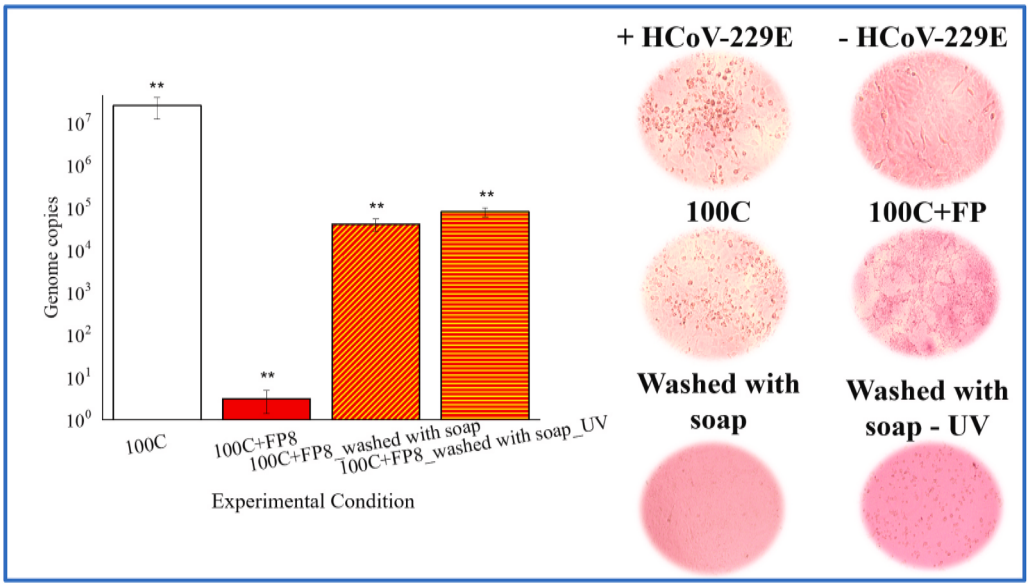

Fig. 4. Virucidal activity of the cotton fabric impregnated with FP (100 C+FP). Viral load (genome copies) of Human Coronavirus 229 (HCoV-229E) detected by qPCR 4 days post-infection and after 5 min of incubation to either 100 C+FP before and after washing with soap or 100 C only. The inset shows representative images of the MRC-5 cells, using a 100X magnification, after 4 days of incubation. One-way ANOVA was used for the statistical analysis with Bonferroni's post-test (**, $P < 0.01$). +HCoV-229E, infected cells; -HCoV-229E, non-infected cells infected with virus exposed to original cotton fabric, cotton fabric with FP, cotton fabric with FP after washing with soap, and cotton fabric with FP after washing and irradiation.

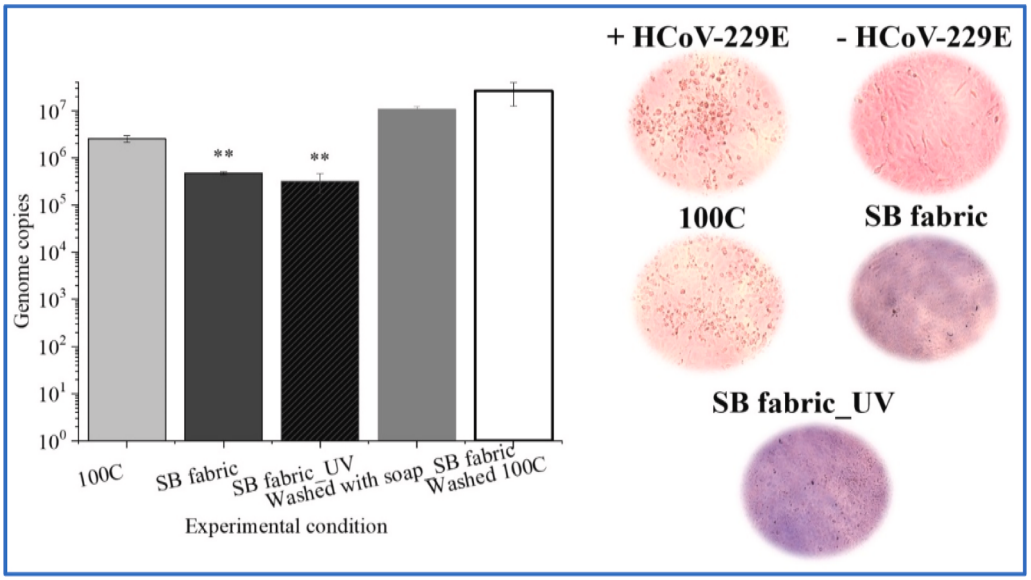

Fig. 5. Virucidal activity of the cotton fabric impregnated with SB (100 C+SB). Viral load (genome copies) of Human Coronavirus 229 (HCoV-229E) detected by qPCR 4 days post-infection and after 5 min of incubation to either 100 C+SB before and after washing with soap or 100 C only. The inset shows representative images of the MRC-5 cells, using a 100X magnification, after 4 days of incubation. One-way ANOVA was used for the statistical analysis with Bonferroni's post-test (**, $P < 0.01$). +HCoV-229E, infected cells; -HCoV-229E, non-infected cells infected with virus exposed to original cotton fabric, cotton fabric with SB, cotton fabric with SB after irradiation.

an enveloped virus used as a model that can be extrapolated to SARS-CoV-2 and other enveloped viruses, as the oxidative damage induced by ROS is a nonspecific mechanism of viral inactivation. The fabrics inoculated with HCoV-229E for 5 min were washed with culture medium and transferred into MRC-5 cells in culture [18]. To warrant that residual FP and SB toxicity should not significantly contribute to MRC-5 cell death, the virucidal assays were preceded by an MTT cell viability assay (Figure S1a and b). MTT is based on the ability of viable cells to metabolically reduce the MTT salt through the succinic mitochondrial dehydrogenase enzyme. The salt reduction promotes the formation of blue-purple formazan crystals that accumulate in the cell cytoplasm [21]. The cell medium used to rinse 100 C+FP and 100 C+SB was added to the MRC-5 cell culture. The cell viability after incubation with the solutions used to rinse 100 C+FP and 100 C+SB was tested using an MTT assay. The results in Figures S1a and b show that residual FP and SB in the rinsing medium did not promote significant cell death. After the fabric washing, the cell viability remained equal to that of the control. The infection by HCoV-229E affects the cell phenotype, as shown in the insets of Figs. 4 and 5 (+HCoV-229E samples versus -HCoV-229E samples). Viral load (copies) of HCoV-229E was detected by qPCR 4 days

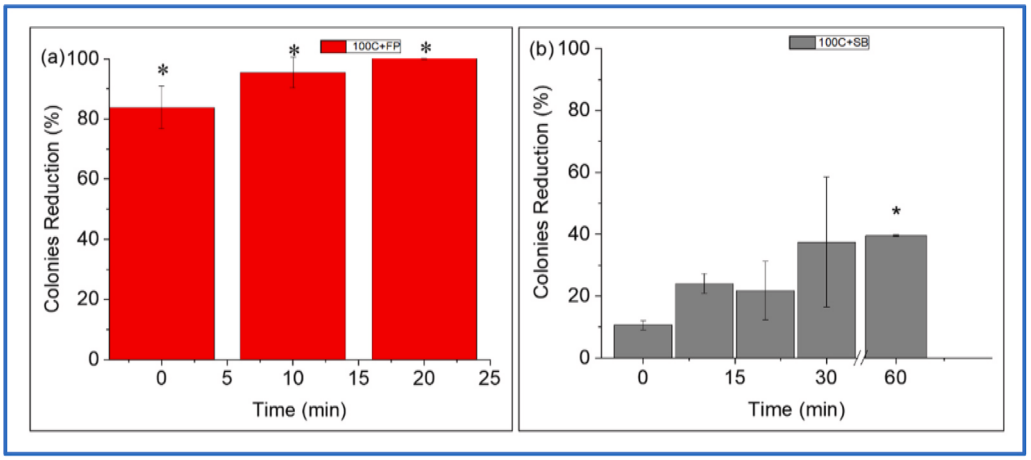

Fig. 6. Percentage of reduction in bacterial colonies after contact with fabrics with (a) FP and (b) SB relative to the control. One-way ANOVA was used for statistical analysis with Bonferroni's post-test (*, $P < 0.05$).

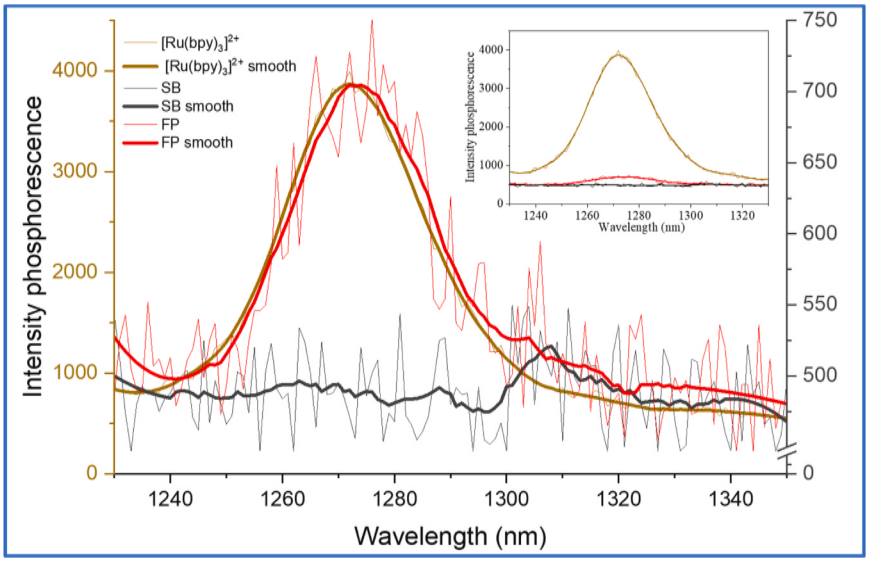

Fig. 7. Sensitized singlet oxygen emission spectra generated by using (a) 100 C+FP (thin and thick red lines) and 100 C+SB (thin and thick black lines) immersed in chloroform and compared to $[Ru(bpy)_3]^{2+}$ (where bpy = 2,2'-bipyridine) in CH_3CN (thin and thick brown lines). The overlapped spectra are on different scales to provide a normalization with a maximum of 1270 nm. The emission intensities of FP and SB (right red and black vertical axes) are only the observed intensities since it was impossible to determine the exact dye quantities in fabrics. The thick lines are the corresponding signal smooth. The inset shows the same results with a single y-axis.

post-infection, and the results are presented in Figs. 4 and 5. The cotton fabric impregnated with FP (Fig. 4) showed an eight-million-fold reduction in the recovered virus compared to the control fabric. After the fabric was washed with soap and dried, it presented a six hundred and thirty percent decrease in the recovered virus compared to the control fabric, yet significantly different from the control. Irradiating the fabric after washing did not increase the virucidal capacity of the fabric. Fig. 5 shows the virucidal results of cotton fabric dyed by SB. The fabric dyed with SB also promoted a significant decrease in virus genome copies relative to 100. Consistent with a higher virucidal effect of FP, washing of 100 C+FP decreased the absorbance and EPR radical cation signals (Figures S2a and b), whereas 100 C+SB retained significantly the UV–visible and EPR signal intensity after washing (Figures S2c and d). These results show that the efficiency of the PTZ virucidal action depends on the dye's availability to contact the viral envelope.

Considering that the PTZs' virucidal action comes from the generation of pro-oxidant species that attack viral envelopes, they also showed promising bactericidal action. 100 C+FP and 100 C+SB were tested against *Escherichia coli* (Fig. 6a and b).

The results of the bactericidal tests reveal that the fabrics dyed with FP and SB exhibit microbicidal properties with varying efficiencies. The 100 C+FP immediately reduced 80 % of the bacterial colonies, whereas 100 C+SB required 1 h of contact to achieve a statistically significant reduction in bacterial colonies. The different microbicidal actions of 100 C+FP and 100 C+SB could result from the production mechanisms of other oxidative species. The radical cations are formed by the type I mechanism [3,7,8]. However, it was essential to investigate whether the type II mechanism also occurred and contributed to the microbicidal action of the PTZs. Fig. 7 shows the spectra of monomol emission of $^1O_2$ produced by different sensitizers in acetonitrile. $[Ru(bpy)_3]^{2+}$ was used as a pattern of photosensitizers with a high yield of $^1O_2$ (brown lines). FP irradiated in acetonitrile generated $^1O_2$ (red line), as shown by the overlap of the spectrum obtained with the standard solution. The acetonitrile SB solution did not exhibit a signal of $^1O_2$ production (black line). The attempts to measure singlet oxygen ($^1O_2$) generated at the 100 C+FP and 100 C+SB surfaces were unfruitful (Figure S3).

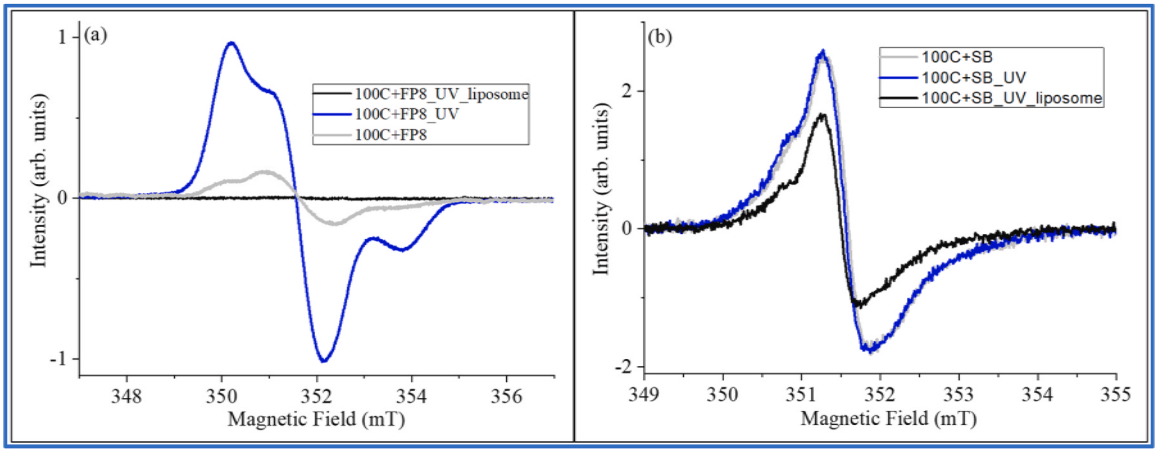

Fig. 8. Reaction of PTZ radical cation with egg yolk PC liposomes. a) EPR spectra of 100 C+FP (light gray line), UV-irradiated 100 C+FP (blue line), and irradiated 100 C+FP immersed in a liposome (black line). b) EPR spectra of 100 C+SB (light gray line), UV-irradiated 100 C+SB (blue line), and irradiated 100 C+SB immersed in a liposome (black line).

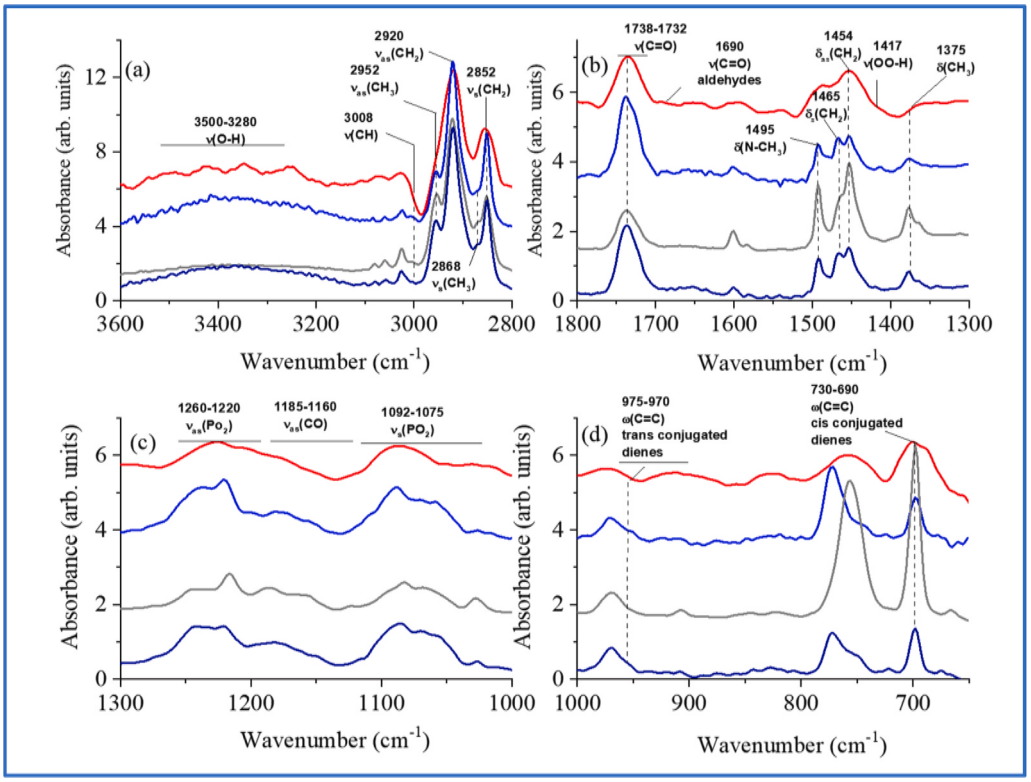

Fig. 9. FTIR analysis of the effect of 100 C+FP on phosphatidylcholine in liposome membrane models. In a), b), c), and d), the panels show the FTIR spectral region of PC pristine in H_2O (dark blue lines) and D_2O (blue lines) and exposed to 100 C+FP (gray and red lines, respectively).

However, these negative results could not be assigned to the absence of singlet oxygen generation in fabrics since $^1O_2$ was not detected in fabrics impregnated with $[Ru(bpy)_3]^{2+}$. The results of lipid damage in liposomes (Figs. 9a-d and b and 10a-d) corroborated that singlet oxygen contributed to the microbicidal action of 100 C+FP. The formation of free radicals and the generation of singlet oxygen by FP and SB suggested that lipid oxidation may be a mechanism contributing to the destruction of viruses and bacteria. Thus, another approach to investigating the mechanism of viruses and bacteria destruction by PTZs was to expose egg yolk PC liposomes to contact with 100 C+FP and 100 C+SB. Phosphatidylcholine (PC) liposomes, a model of the lipid fraction of the viral envelope and bacterial membrane, were used to study the oxidation promoted by fabric with FP and SB (Figs. 8a and b, 9a-d and 10a-d). The PC liposomes were exposed to cotton fabrics impregnated with FP and dyed with SB employing an industrial process. Before and after contact with the fabrics, the samples were analyzed by EPR and FTIR.

Fig. 8a shows that the contact of PC liposomes with cotton fabric impregnated with FP and irradiated with a UV lamp significantly decreased the EPR signal of FP radical cation, indicating the reaction of the pro-oxidant species with lipid molecules. Consistent with the less intense virucidal and bactericidal effects, a less intense decay of the EPR signal of cotton fabric dyed with SB was observed after liposome exposure (Fig. 8b). FTIR was also used to analyze the samples of

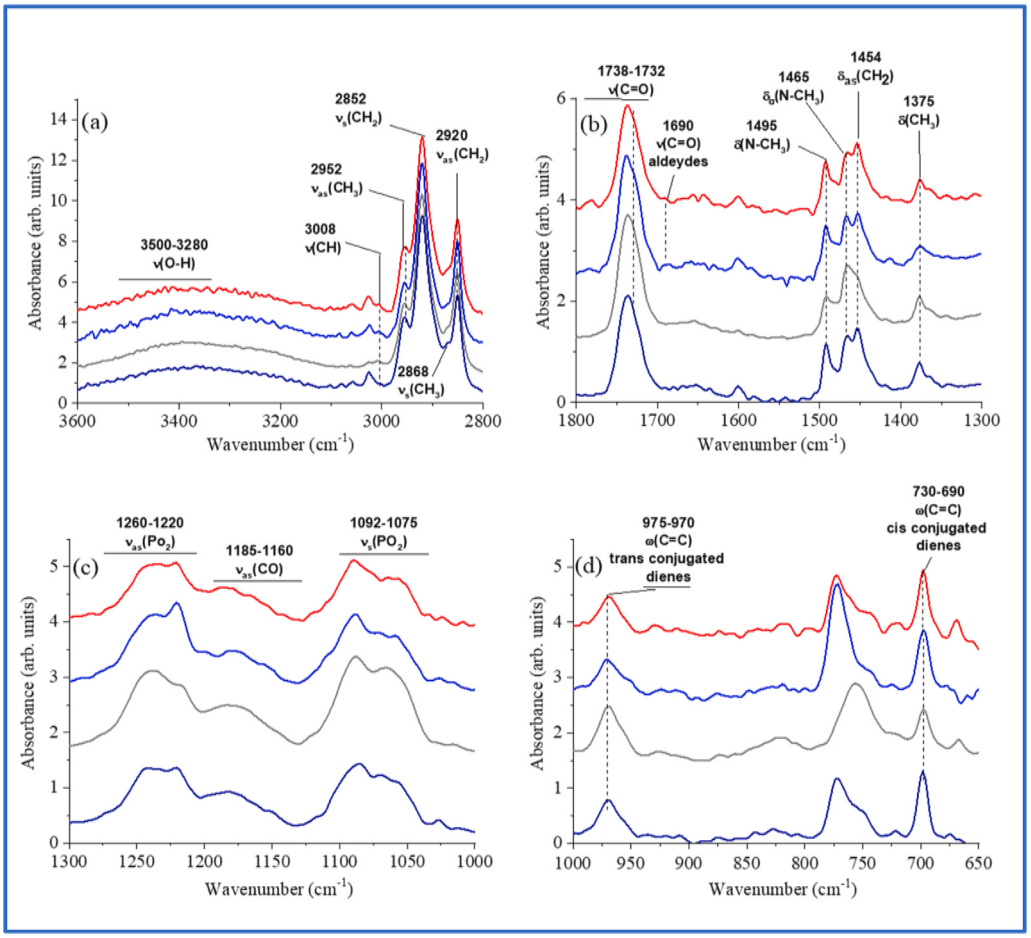

Fig. 10. FTIR analysis of the effect of 100 C+SB on phosphatidylcholine in liposome membrane models. In a), b), c), and d), the panels show the FTIR spectral region of PC pristine in H_2O (dark blue lines) and D_2O (blue lines) and exposed to 100 C+SB (gray and red lines, respectively).

liposomes exposed to contact with 100 C+FP and 100 C+SB (Figs. 9a-d and 10a-d, respectively). For FTIR analysis, PC liposomes in deuterium oxide (D_2O) were also prepared to investigate the participation of singlet oxygen in lipid damage (Figs. 9c-d and 10c-d). Fig. 9a-d shows changes in the vibrational bands of PC after exposure to FP-treated cotton fabric, with different results for the samples prepared in water and deuterium oxide. The PC liposomes prepared in deuterium oxide and exposed to FP in cotton fabric exhibited a broadening of all vibrational bands. This result indicates a significant increase in the sample fluidity due to oxidative damage and lipid degradation.

Before exposure to oxidative species, PC liposomes prepared in water and deuterium oxide exhibited vibrational bands related to the lipid functional groups. In the spectral region of 3600–3300 cm^{-1}, the contribution of OH and NH stretching is observed. After exposure to FP-treated cotton fabric, PC liposome presented higher bands below 3300 $cm^{-1,}$ consistent with increased lipid hydroperoxides. Within the spectral region of 3100–2800 cm^{-1}, the expected contribution of CH, CH_2, and CH_3 stretching is evidenced. In the area of 1800–1300 cm^{-1}, the band peaking at 1735 cm^{-1} is assigned to the stretching vibration of ester carbonyl groups. The decrease of these bands in PC liposomes after oxidation is consistent with lipid fragmentation in the terminal step of lipid peroxidation (see steps of lipid oxidation in Fig. 11). In the 1300 to 1000 cm^{-1} region, where the vibrations of phosphate groups are found, more significant changes were observed in the samples prepared in D_2O.

These results indicate a substantial contribution of singlet oxygen. The oxidation of the lipid acyl chain and the formation of lipid hydroperoxides significantly affect lipid packing and have repercussions on the lipid head groups. In the spectral region of 1000 to 700 cm^{-1}, a significant increase in the signals associated with cis-conjugated dienes was observed. The intensification of cis-conjugated diene signals was higher in the sample prepared in water than in D_2O, suggesting a competition between the oxidative attack by free radicals and singlet oxygen. Consistent with the less efficient virucidal and bactericidal effects, the EPR signal and changes in vibrational bands of liposomes exposed to cotton fabric dyed with SB were less intense. Significant band broadenings were not observed in the liposomes prepared in D_2O after exposure to 100 C+SB, reinforcing that band broadening resulted from lipid damage and not an intrinsic effect of D_2O on liposomes.

4. Conclusion

In conclusion, the findings presented in this article demonstrate that fabric dyes containing phenothiazine moieties exhibit photoactivated microbicidal action against viruses and bacteria, providing a guide for developing new phenothiazines for use as microbicidal dyes. The analysis of fabric impregnation with FP and SB dyeing, conducted using UV–visible and EPR techniques, was consistent with the successful impregnation of the PTZs in the fabrics. The virucidal and bactericidal properties of fabrics impregnated with FP and SB highlight the potential of fabrics impregnated with PTZs as self-disinfecting materials, offering a promising avenue for combating the spread of pathogens. In this regard, the present study is the first account of the microbicidal action of an industrial dye. Another significant contribution of the present study was demonstrating that the microbicidal action of PTZs has a structural dependence related to the degree of impregnation and sensitization of molecular oxygen to the singlet excited state. Additionally, the results

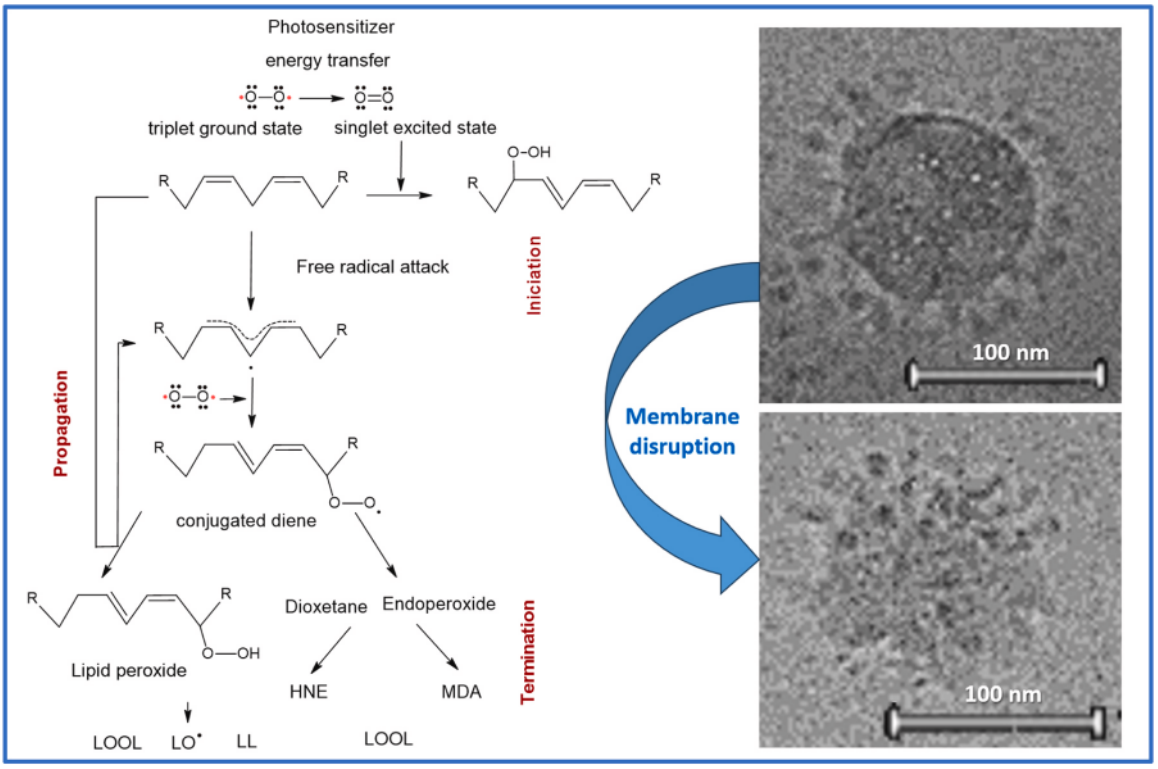

Fig. 11. Free radicals and singlet molecular oxygen promote the main steps of lipid oxidation. The right panel shows Cryomicroscopy images of whole and destroyed coronavirus after exposure to phenothiazine radical cation.

demonstrated the importance of using non-specific pro-oxidant agents because they provide broad efficacy against various viruses and bacteria, underscoring the versatility and utility of these treated fabrics.

Several points that were not contemplated in the present study can be addressed in future studies about the microbicidal action of photoactivated phenothiazines, such as:

- Synthesis of different phenothiazine derivative dyes and other aromatic dyes that can generate stable radical cations and singlet oxygen upon irradiation.
- Synthesis of a dye containing a phenothiazine moiety that should be appropriate for synthetic fibers.
- Association of phenothiazine dyed fabrics with metallic nanoparticles, with overlapping of dye luminescence (fluorescence and dimol singlet oxygen emission) with the surface plasmon resonance band of the nanoparticles, a strategy with potential to intensify microbicidal action.
- The application of phenothiazine compounds, alone and in association, against non-enveloped viruses and the H5N1 virus that has the potential to lead to a new pandemic.

CRediT authorship contribution statement

Lilian Martins-Nascimento: Writing – review & editing, Writing – original draft, Validation, Methodology, Investigation, Data curation, Conceptualization. **Carin Cristina S. Batista:** Methodology, Formal analysis, Data curation, Conceptualization. **Luiza F. Sobrinho:** Methodology, Formal analysis. **Adrianne M.M. Brito:** Methodology, Formal analysis. **Juliana D. Bronzato:** Methodology, Formal analysis. **Martha T. Oliveira:** Original draft, Methodology, Formal analysis. **Karina P. M. Frin:** Original draft, Methodology, Formal analysis. **Silgia A. Costa:** Writing – original draft, Methodology, Formal analysis, Data curation. **Sirlene M. Costa:** Writing – original draft, Methodology, Investigation, Data curation. **Otaciro R. Nascimento:** Writing – original draft, Methodology, Investigation, Formal analysis, Data curation. **Iseli L. Nantes:** Writing – review & editing, Supervision, Project administration, Funding acquisition, Formal analysis, Conceptualization.

Declaration of Competing Interest

Lilian Martins-Nascimento, Carin Cristina S. Batista, Luiza F. Sobrinho, Juliana D. Bronzato, Martha T. Oliveira, Karina P. M. Frin Adrianne M. M. Brito, Silgia A. Costa, Sirlene M. Costa, Otaciro R. Nascimento, and Iseli L. Nantes declare no conflict of interest.

Acknowledgments

The authors thank Fundação de Amparo à Pesquisa do Estado de São Paulo (FAPESP, 2017/02317-2 and 2017/25090-3), Coordenação de Aperfeiçoamento de Pessoal de Nível Superior (CAPES, 88887.513142/2020-00), Conselho Nacional de Desenvolvimento Científico e Tecnológico (CNPq, 313111/2021-9) for financial support, UFABC Multi-User Experimental Central (CEM/UFABC) and National Laboratory of Nanotechnology (LNNano) of National Energy and Materials Research Center (CNPEM) for access to facilities.

Appendix A. Supporting information

Supplementary data associated with this article can be found in the online version at doi:10.1016/j.nxmate.2025.101125.

References

[1] G. Pullangott, U. Kannan, G. S, D.V. Kiran, S.M. Maliyekkal, A comprehensive review on antimicrobial face masks: an emerging weapon in fighting pandemics, RSC Adv. 11 (2021) 6544–6576, https://doi.org/10.1039/d0ra10009a.
[2] F. Seidi, C. Deng, Y. Zhong, Y. Liu, Y. Huang, C. Li, H. Xiao, Functionalized masks: powerful materials against COVID-19 and future pandemics, Small 17 (2021) 1–24, https://doi.org/10.1002/smll.202102453.

[3] L.S. Martins-Nascimento, A.M.M. Brito, J.D. Bronzato, M.T. Oliveira, S.A. Costa, S. M. Costa, O.R. Nascimento, I.L. Nantes, Virucidal action of photogenerated pink phenothiazine radical cation impregnated in cotton fabric and polypropylene face mask, J. Photochem. Photobiol. A Chem. 445 (2023) 115110, https://doi.org/10.1016/j.jphotochem.2023.115110.
[4] C.A. Fabio, M.B. Yolanda, G.M. Carmen, C. Francisco, B. Antonio Julián, P. L. Leonor, S. Jesús, Use of photodynamic therapy and chitosan for inactivacion of candida albicans in a murine model, J. Oral. Pathol. Med. 45 (2016) 627–633, https://doi.org/10.1111/jop.12435.
[5] J. Vara, M.S. Gualdesi, S.G. Bertolotti, C.S. Ortiz, Two phenothiazine dyes as photosensitizers for the production of singlet oxygen. Photophysics, photochemistry and effects of aggregation, J. Mol. Struct. 1181 (2019) 1–7, https://doi.org/10.1016/j.molstruc.2018.12.078.
[6] J.A. Christensen, B.T. Phelan, S. Chaudhuri, A. Acharya, V.S. Batista, M. R. Wasielewski, Phenothiazine radical cation excited states as super-oxidants for energy-demanding reactions, J. Am. Chem. Soc. 140 (2018) 5290–5299, https://doi.org/10.1021/jacs.8b01778.
[7] T. Rodrigues, C.G.Dos Santos, A. Riposati, L.R.S. Barbosa, P. Di Mascio, R. Itri, M. S. Baptista, O.R. Nascimento, I.I. Nantes, Photochemically generated stable cation radical of phenothiazine aggregates in mildly acid buffered solutions, J. Phys. Chem. B 110 (2006) 12257–12265, https://doi.org/10.1021/jp0605404.
[8] H.F. Santos, C.G. dos Santos, O.R. Nascimento, A.K.C.A. Reis, A.J.C. Lanfredi, H.P. M. de Oliveira, I.L. Nantes-Cardoso, Charge separation of photosensitized phenothiazines for applications in catalysis and nanotechnology, Dyes Pigments 177 (2020) 108314, https://doi.org/10.1016/j.dyepig.2020.108314.
[9] M. Garcia-Diaz, Y.Y. Huang, M.R. Hamblin, Use of fluorescent probes for ROS to tease apart type I and type II photochemical pathways in photodynamic therapy, Methods 109 (2016) 158–166, https://doi.org/10.1016/j.ymeth.2016.06.025.
[10] C.H. Wu, L.Y. Bai, M.H. Tsai, P.C. Chu, C.F. Chiu, M.Y. Chen, S.J. Chiu, J. H. Chiang, J.R. Weng, Pharmacological exploitation of the phenothiazine antipsychotics to develop novel antitumor agents-a drug repurposing strategy, Sci. Rep. 6 (2016) 1–11, https://doi.org/10.1038/srep27540.
[11] M. Otręba, A. Beberok, D. Wrześniok, E. Buszman, In vitro melanogenesis inhibition by fluphenazine and prochlorperazine in normal human melanocytes lightly pigmented, DARU J. Pharm. Sci. 26 (2018) 85–89, https://doi.org/10.1007/s40199-018-0206-4.
[12] C.J. Wiley, Sulfur Dyes 1 (2004) 1873.
[13] K. Hunger, P. Gregory, P. Miederer, H. Berneth, C. Heid, W. Mennicke, Important Chemical Chromophores of Dye Classes, 2002. https://doi.org/10.1002/35276 02011.ch2.
[14] J.N. Chakraborty, Sulphur dyes, Woodhead Publishing Limited (2011), https://doi.org/10.1533/9780857093974.2.466.
[15] R. Christie, Azo Dyes and Pigments, 2023. https://doi.org/10.1039/bk 9781849733281-00072.
[16] X. Song, J. Padrão, A.I. Ribeiro, A. Zille, Testing, characterization and regulations of antimicrobial textiles. Antimicrobial Textiles from Natural Resources, Elsevier, 2021, pp. 485–511, https://doi.org/10.1016/B978-0-12-821485-5.00012-3.
[17] G.G.D.E. Toledo, V.H. Toledo, A.J.C. Lanfredi, M. Escote, A. Champi, M.C.C. Da Silva, I.L. Nantes-Cardoso, Promising nanostructured materials against enveloped virus, Acad. Bras. Cienc. 92 (2020) 1–22, https://doi.org/10.1590/0001-3765202020200718.
[18] J.D. Bronzato, A. Tofanello, M.T. Oliveira, J. Bettini, A.M.M. Brito, S.A. Costa, S. M. Costa, A.J.C. Lanfredi, O.R. Nascimento, I.L. Nantes-Cardoso, Virucidal, photocatalytic and chiromagnetic cobalt oxide quantum dots, Appl. Surf. Sci. 576 (2022) 151847, https://doi.org/10.1016/j.apsusc.2021.151847.
[19] R. Rathnasinghe, S. Jangra, L. Miorin, M. Schotsaert, C. Yahnke, A. García-Sastre, The virucidal effects of 405 nm visible light on SARS-CoV-2 and influenza a virus, Sci. Rep. 11 (2021) 1–10, https://doi.org/10.1038/s41598-021-97797-0.
[20] P.D. Rakowska, M. Tiddia, N. Faruqui, C. Bankier, Y. Pei, A.J. Pollard, J. Zhang, I. S. Gilmore, Antiviral surfaces and coatings and their mechanisms of action, Commun. Mater. 2 (2021) 1–19, https://doi.org/10.1038/s43246-021-00153-y.
[21] C.C.S. Batista, L.J.C. Albuquerque, I. De Araujo, B.L. Albuquerque, F.D. Da Silva, F. C. Giacomelli, Antimicrobial activity of nano-sized silver colloids stabilized by nitrogen-containing polymers: the key influence of the polymer capping, RSC Adv. 8 (2018) 10873–10882, https://doi.org/10.1039/c7ra13597a.
[22] E. Pinho, L. Magalhães, M. Henriques, R. Oliveira, Antimicrobial activity assessment of textiles: standard methods comparison, Ann. Microbiol. 61 (2011) 493–498, https://doi.org/10.1007/S13213-010-0163-8/FIGURES/4.
[23] E. Pinho, G. Soares, M. Henriques, M. Grootveld, Antibacterial Activity of Textiles for Wound Treatment, Https://Doi.Org/10.14504/Ajr.2.5.1 2 (2015) 1–7. https://doi.org/10.14504/AJR.2.5.1.